Composite Structures 268 (2021) 113974

Contents lists available at ScienceDirect

Composite Structures

journal homepage: www.elsevier.com/locate/compstruct

3D printed recoverable honeycomb composites reinforced by continuous carbon fibers

Yunyong Cheng [a], Junjie Li [a], Xiaoping Qian [b], Stephan Rudykh [b,*]

[a] School of Mechanical Engineering, Northwestern Polytechnical University, Xi'an, Shaanxi 710072, China
[b] Department of Mechanical Engineering, University of Wisconsin-Madison, WI 53706, USA

ARTICLE INFO

Keywords:
3D printing
Continuous carbon fiber
Honeycomb composites
Recoverability
Energy absorption

ABSTRACT

This paper reports the failure and recovery mechanisms of 3D-printed lightweight honeycomb composites. Through this experimental study, we demonstrate the enhanced mechanical performance of 3D-printed composite structures and their ability for shape recovery under heat excitation. The remarkable mechanical performance of the reinforced honeycombs draws from the combination of the structural geometry and the tailored material composition. The results show that the addition of continuous fibers enables the honeycomb structure to avoid catastrophic failure even at high levels of deformation, which allows the shape memory effect to be activated and nearly 87% percent of the initial structural shape to be recovered. Moreover, the reinforced honeycombs exhibit enhanced properties: the specific energy absorption and specific stiffness of the reinforced honeycombs are up to 2 times greater than those of the conventional honeycombs. These enhanced mechanical properties combined with the controllable shape recovery of the 3D-printed structures can be used in the design of novel energy absorbing and protective material systems, biomedical devices, and actuators.

1. Introduction

Honeycomb structures are lightweight cellular structures that have been widely adopted as sandwich panel cores, energy absorbers, vibration dampers and insulators in the aerospace, automotive and civil engineering fields due to their light weight, novel thermomechanical properties and energy absorption capability [1–5].

Three-dimensional printing technology has the ability to fabricate very complex, even arbitrary structures, and has already been applied to print cellular functional structures, including ultraelastic hierarchical foams [6], ultralight metallic microlattices [7], hierarchical porous ceramics [8] and honeycombs, such as regular honeycombs [9–13], density-graded honeycombs [14], hierarchical honeycombs [15] and multimaterial honeycombs [16].

Fiber-reinforced polymer 3D printing can significantly enhance the mechanical properties of printed polymer specimens; in particular, when continuous fiber is used as the reinforcement phase, this mechanical property enhancement will be even more obvious. Continuous fiber-reinforced polymer 3D printing has begun to be investigated in recent years and is getting more and more attention [17]. A few studies have focused on the fabrication and mechanical property testing, including tension, bending, and compression tests, of continuous fiber-reinforced 3D-printed standard specimens [18–20]. Continuous fibers play a role in the reinforcement phase, including continuous carbon fibers [21 23–31], Kevlar fibers [22–23], glass fibers [23–25] and jute fibers [26]. Polymers that typically act as matrix phases include Nylon [21–26], polylactide (PLA) [26–29 31] and acrylonitrile butadiene styrene (ABS) [30].

Some more complex composite structures fabricated via continuous carbon fiber-reinforced 3D printing technology have also been reported, including corrugated structures [32] and sandwich structures with honeycomb, rhombus, rectangle, and circle core shapes [33,34]. The continuous carbon fiber reinforcement notably improved the mechanical properties of these structures. The failure mechanism and modeling methods of composites including 3D printed bio-inspired structures has also been to be discussed [35–37].

Here, we present a lightweight, recoverable, continuous carbon fiber-reinforced PLA honeycomb composite structure (Fig. 1(a)) with a novel energy absorption capability, which was fabricated using a modified fused filament fabrication (FFF) 3D printing device. Through experiments, we show that the 3D-printed honeycomb composite structures integrate the advantages of the excellent mechanical properties of the continuous carbon fibers, the deformation mechanism of honeycomb structures. As the honeycomb structural integrity was pre-

* Corresponding author.
E-mail address: rudykh@wisc.edu (S. Rudykh).

https://doi.org/10.1016/j.compstruct.2021.113974
Received 24 September 2020; Revised 24 March 2021; Accepted 7 April 2021
Available online 16 April 2021

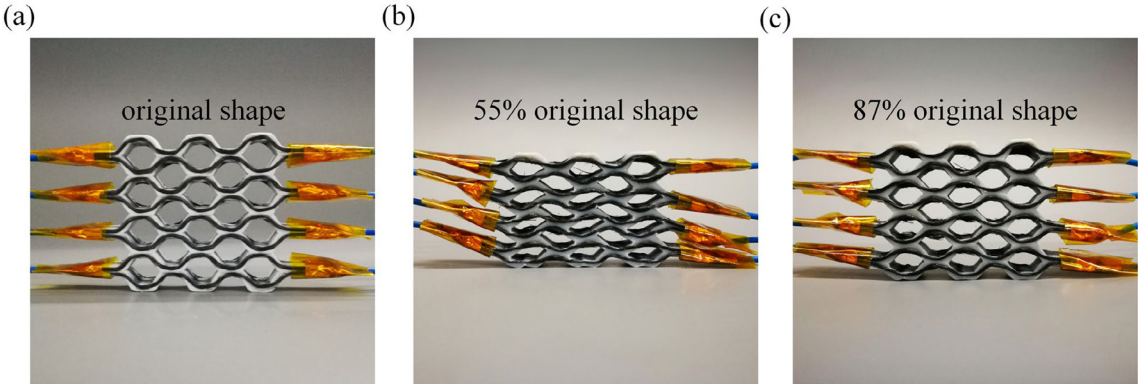

Fig. 1. 3D-printed recoverable PLA honeycomb structure reinforced by continuous carbon fibers: (a) original shape of the printed honeycomb structure, (b) compressed honeycomb structure with $\varepsilon = 0.45$, and (c) recovered honeycomb structure acquired by applying 5 V for 5 min.

served well after compression testing under certain load direction, we further investigated the recovery property of the compressed honeycomb structure based on the thermally induced polymer shape memory effect of PLA matrix.

In the considered 3D-printed honeycomb composite structure, the continuous carbon fiber serves as two roles: one as the reinforcement phase and the other as a heat generator for activation of the shape memory effect. Through the electric resistance of the continuous carbon fiber, the applied voltage can be converted into heat to excite the shape memory effect of the polymer matrix [38–46]. It was found that the severely deformed composite structures can recover nearly to their initial shape upon low voltage electrical excitation. Fig. 1 illustrates the effect on the original shape of 3D-printed fiber-reinforced honeycomb (a), compressed honeycomb with large compressive strain (55% of its initial shape) (b), and restored shape (87% of its initial shape) of the honeycomb structure due to the electrical excitation of 5 V voltage (c).

2. Materials and methods

2.1. Honeycomb fabrication

To fabricate the composite honeycombs, a custom-made 3D printer (based on a commercial FFF platform) was used. The modified material fabrication platform allows us to print the continuous fiber-reinforced honeycomb structures with a continuous carbon fiber bundle (HTA 40, Toho Tenax Co., Ltd, Japan) as the reinforcement phase and a PLA filament (FlashForge, Hangzhou, Zhejiang, China) as the matrix phase. The properties of the adopted HTA 40 carbon fiber bundle (containing 1000 single carbon fibers) and the PLA filament are summarized in Table 1.

The schematics of the 3D printing process are shown in Fig. 2(a). PLA is heated in the heat chamber and turns into a semifluid state, after which in situ impregnation of the carbon fiber bundle with the thermoplastic occurred. Under the internal pressure of the extrusion head, the semifluid thermoplastic and continuous carbon fibers are extruded from the nozzle tip and adhere to the heat bed or former layers (Fig. 2(b)). The average width of the carbon fiber bundle is approximately 0.9 mm, and the tip diameter of the extrusion head is 1.5 mm.

Fig. 3(b) shows the geometries of the printed unit cells, wherein the geometrical parameters defining the structures are the thicknesses of the honeycomb links t_1 and t_2, their lengths h and l, and the characteristic angle θ. The loading directions for longitudinal and transverse compression testing are defined in Fig. 3(c) and (d), respectively. Based on the geometrical parameters the relative density is defined as

$$\Delta\rho = \frac{ht_1 + 2lt_2}{2hl\sin\theta + l^2\sin 2\theta} \tag{1}$$

The carbon fiber content is calculated as follows

$$\omega_c = \frac{W_{carbon}}{W_{matrix}} = \frac{2(h+l)\rho_c}{(ht_1 + 2lt_2)H_l\rho_s} \tag{2}$$

For the case $t_1 = 2\,t_2$, Eq. (2) reduces to

$$\omega_c = \frac{\rho_c}{t_2 H_l \rho_s} \tag{3}$$

here W_{carbon} and W_{matrix} represent the weight of the carbon fiber and matrix material, respectively; and ρ_s, ρ_c, and H_l are the density of the matrix, linear density of the carbon fiber and layer height of the specimens, respectively. Additional details for the relative density calculation are given in Appendix A.

The dimensions of the honeycomb structure for compression testing are shown in Fig. 4(a). To facilitate 3D printing of continuous fiber-reinforced honeycomb structures, additional auxiliary structures were added to the honeycomb structures, as shown in Fig. 4(b). The original 3D-printed honeycomb structure is shown in Fig. 4(c). The final honeycomb structure for compression testing after cutting off the additional auxiliary structure is shown in Fig. 4(d).

The contact resistance between the electric cable and the carbon fiber-reinforced honeycombs has a significant influence on the self-heating performance. To obtain a reasonable result, some processing steps were adopted to fabricate honeycomb samples for the heat stimulating recovery experiments, as shown in Fig. 5. The original 3D-printed carbon fiber-reinforced structure is shown in Fig. 5(a). The honeycomb structure after cutting off the extra 3D printing assisting

Table 1
Mechanical properties of carbon fiber and PLA.

	Tensile strength	Tensile modulus	Elongation at break	Density
HTA 40	4100 MPa	240 GPa	1.7%	1.77g/cm^3
PLA filament	62.63 MPa	3.2 GPa	4.43%	1.24g/cm^3

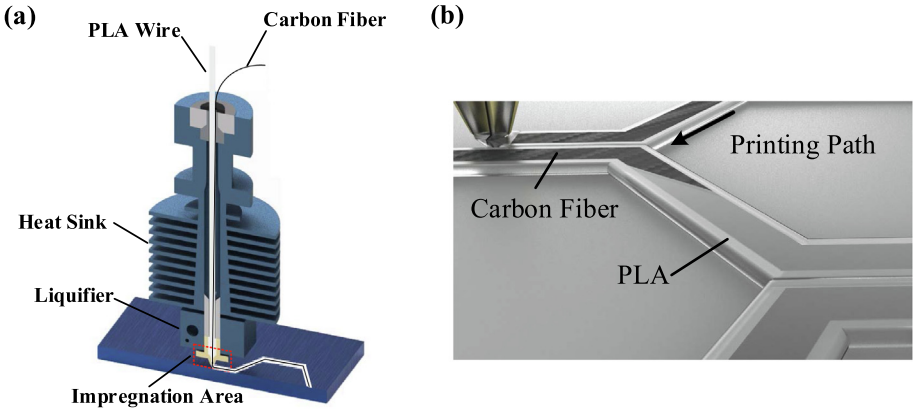

Fig. 2. 3D printing of carbon fiber-reinforced honeycomb: (a) the setup of the modified 3D printer and (b) a schematic presentation of the printing process of carbon fiber-reinforced honeycomb.

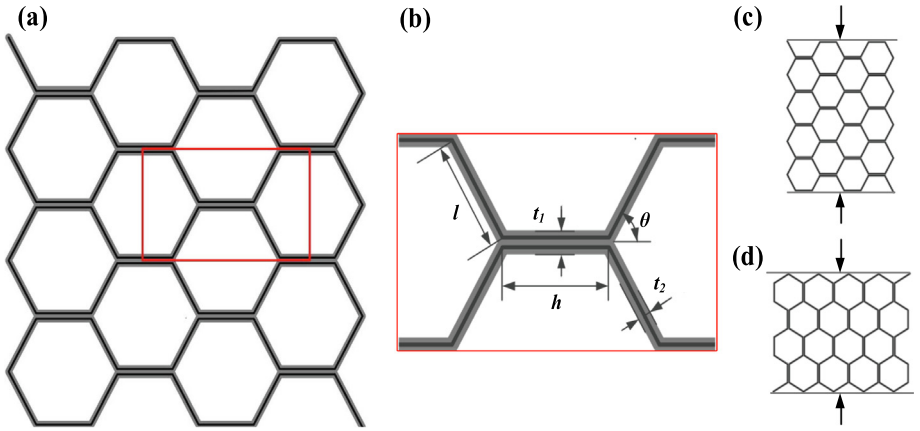

Fig. 3. Carbon fiber-reinforced honeycomb: (a) honeycomb sketch, (b) unit cell geometry, (c) longitudinal loading direction, and (d) transverse loading direction.

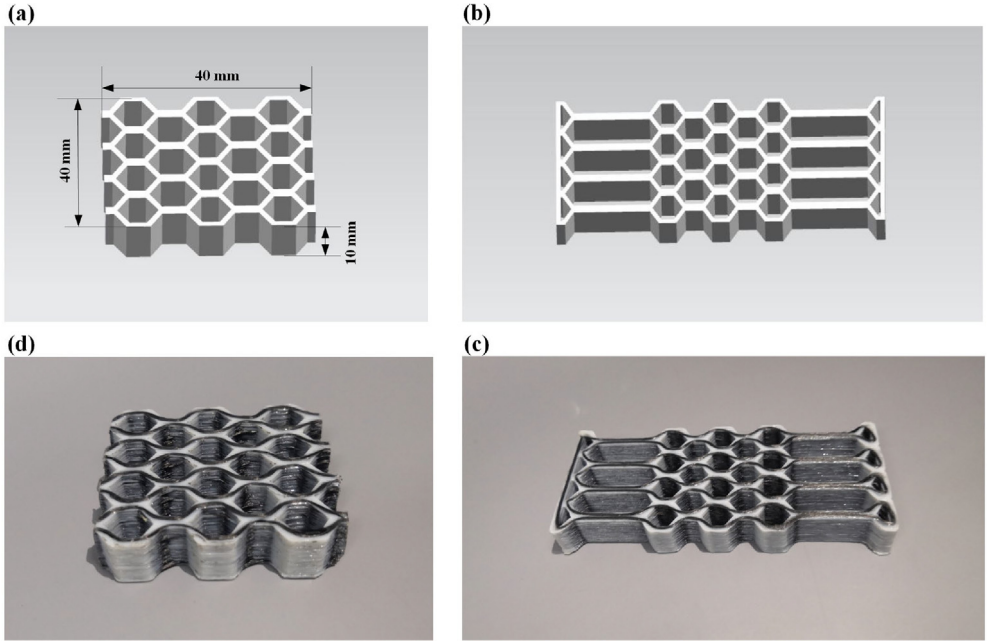

Fig. 4. 3D-printed continuous carbon fiber-reinforced honeycomb specimen for compression testing: (a) the dimensions of the honeycomb structure for compression testing, (b) the designed honeycomb structure with extra 3D printing assisting structure, (c) the original 3D-printed honeycomb structure, and (d) the final honeycomb structure for compression testing.

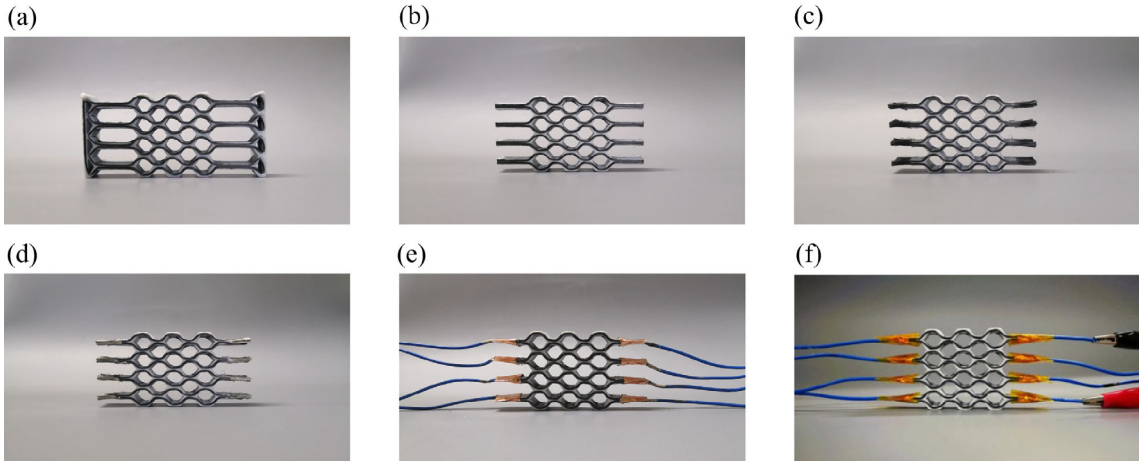

Fig. 5. Preparation process of the 3D-printed continuous carbon fiber-reinforced honeycomb specimen: (a) original 3D-printed continuous carbon fiber-reinforced honeycomb structure, (b) cutting off the printing assisting portions on both sides of the original honeycomb, (c) removal of the PLA matrix material from both sides of the honeycomb structure, (d) coating the exposed carbon fiber bundle with conductive epoxy resin, (e) connecting cable wires to the silver paste-coated carbon fibers and winding copper foil on the outside of the fibers to prevent the wires from falling off during compression testing, and (f) winding high-temperature insulating tape on the outside of the copper foil to prevent possible short-circuits during compression testing.

portion is shown in Fig. 5(b). As the matrix is electrically insulating and completely surrounds the carbon fiber, the honeycomb edges were partially burned to expose the carbon fiber, which was coated with the polymer matrix, and the exposed carbon fiber was sanded with 200 grit sandpaper to remove the remaining matrix, as shown in Fig. 5 (c). To reduce the contact resistance and prevent heat from accumulating at the electrical contact, the carbon fiber was coated with conductive silver epoxy and covered with copper foil to protect the carbon fiber, as shown in Fig. 5(d) and (e). Then, each row of honeycombs was cascaded with copper wire to form a series of circuits; hence, the current can run through the whole honeycomb structure, as shown in Fig. 5(f).

2.2. Mechanical testing

The compression tests were performed using a universal testing machine (INSTRON 3382) with a 100 kN load cell. The tests were conducted at a quasistatic strain rate of $0.001 s^{-1}$. For all specimens, multiple experiments were performed, and the average response along with the standard deviation were reported. Since the structures exhibit different responses when loaded in longitudinal and transverse directions, the corresponding testing was performed, as schematically shown in Fig. 3(c) and (d), respectively. The deformation process was captured by a high-resolution camera (Basler acA1600-20gc, Basler AG, Ahrensburg, DE) at a 1 Hz frequency.

3. Results and discussion

3.1. Mechanical properties under compressive loading

3.1.1. Comparison with conventional honeycombs

We start by reporting the mechanical response of the reinforced structure to compressive loading. Fig. 6(a) shows typical mechanical responses of conventional honeycombs and reinforced honeycombs under longitudinal or traverse loads. The reinforced honeycombs and regular honeycombs are characterized by identical relative density values of 0.31, the fiber content of the reinforced honeycombs is about 14% by volume.

Fig. 6(a) shows that the stress–strain curves of the conventional honey combs exhibit a significant decrease in stress after reaching the peak stress; this phenomenon is mainly due to the buckling and brittle fracture of the cell walls. Reinforced honeycombs have higher mechanical properties than conventional honeycombs; however, the performance of reinforced honeycombs varies under different loading directions. When reinforced honeycombs are subjected to a transverse load, the mechanical response is similar to that of conventional honeycombs. When reinforced honeycombs are subjected to a longitudinal load, the stress–strain curve is remarkably smooth and stable. Its stress–strain curve can be divided into three stages: linear elasticity stage, plateau stage and densification stage.

We summarized the specific stiffness and specific energy absorption (SEA) in Fig. 6(b,c). Three samples of each kind of printed honeycomb were tested. The specific stiffness is calculated as $E_S = \frac{E}{\rho} = \frac{E}{\Delta\rho\rho_s}$, and SEA is calculated as $SEA = \frac{\int_0^d F(\delta)d\delta}{m} = \frac{\int_0^\varepsilon \sigma(\varepsilon)d\varepsilon}{\Delta\rho\rho_s}$.

Clearly, the compressive strength and energy absorption of the reinforced honeycombs are significantly higher than those of the conventional honeycombs. In particular, the reinforced honeycombs under traverse loading exhibit the highest specific stiffness of 425 kN·m/kg, which is 2.6 times that of the corresponding conventional honeycomb under transverse loading.

Although the fiber-reinforced structures show enhanced mechanical properties in both directions, the longitudinal direction benefits the most because the stiffness of carbon fiber can be utilized more effectively in this configuration.

Interestingly, however, the maximum SEA and normalized strength are achieved by the specimens under longitudinal loading, and these values are 5.32 J/g and 10.74 kN·m/kg, respectively. The stress–strain curve of the reinforced honeycomb under longitudinal loading is smoother than that in the transverse direction. This phenomenon can be explained by the different failure modes between each honeycomb and the desirable properties of carbon fibers, which will be discussed in detail in section 3.2.

3.1.2. Influence of relative density on the mechanical performance

Next, we examined the influence of the relative density on the mechanical performance of the reinforced honeycomb structure. To this end, several specimens with identical carbon fiber content (14%) and relative densities varying from 0.22 to 0.40 were fabricated and tested. Fig. 7 shows the responses of reinforced honeycombs under compression.

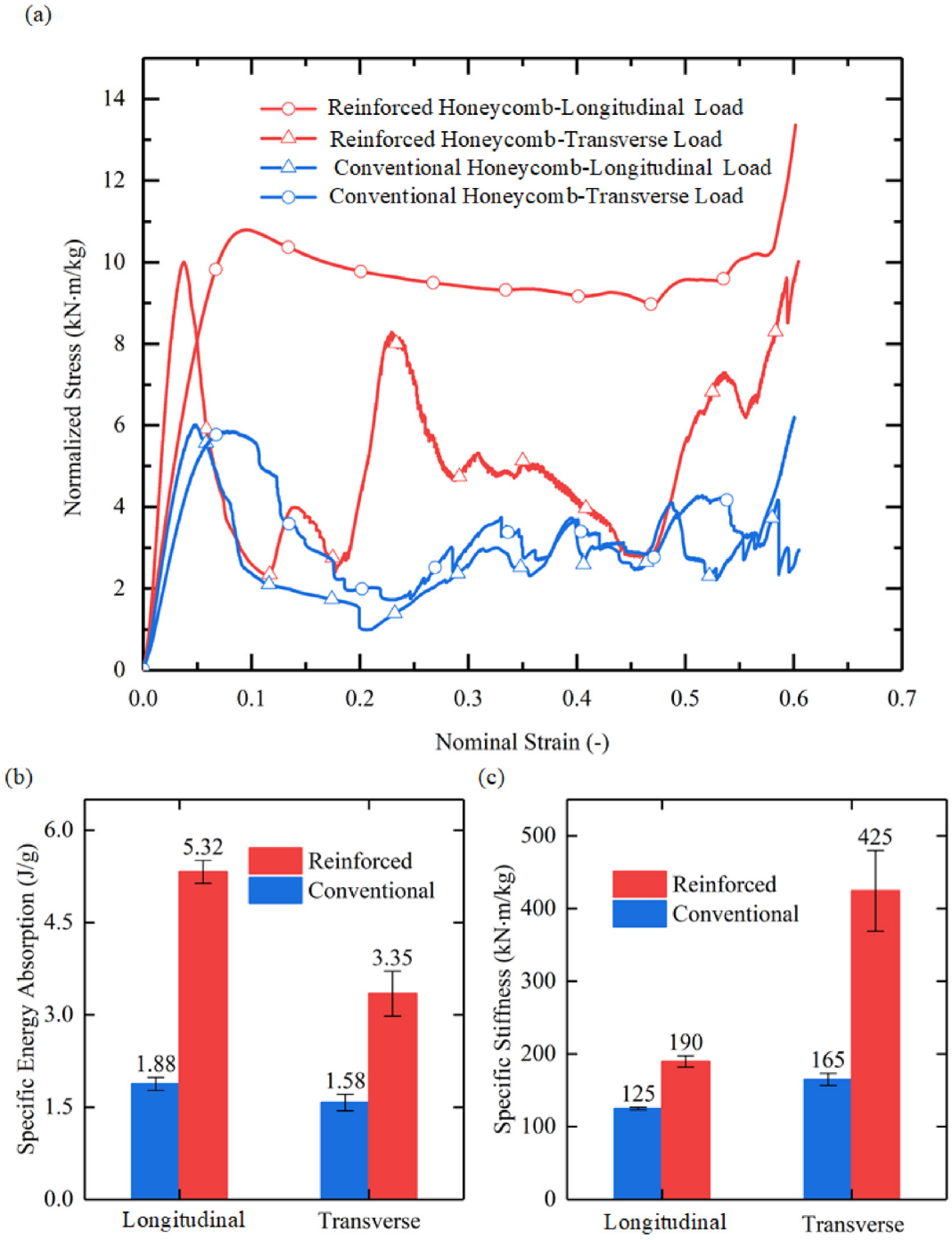

Fig. 6. Mechanical response of carbon fiber-reinforced honeycombs and conventional honeycombs in longitudinal and transverse loading directions: (a) normalized stress–strain curves of conventional honeycombs and reinforced honeycombs and a (b)-(c) comparison of the specific energy absorption and specific stiffness between reinforced honeycombs and conventional honeycombs.

Fig. 7(a) shows that the stress–strain curves become more stable with increasing relative density, and the strain required for the honeycombs to enter the densification stage decreases gradually as the relative density increases, leading to a significant increase in the strength of the honeycombs. We summarize the effect of relative density on SEA, specific stiffness and specific strength of honeycombs in Fig. 7(b). When the relative density increases from 0.22 to 0.40, the SEA of honeycombs increases from 2.69 J/g to 8.32 J/g, the specific stiffness of the honeycombs increases from 68.15kN · m/kg to 245.73kN · m/kg, and the specific strength of the honeycombs increases most notably from 5.80 kN · m/kg to 39.95 kN · m/kg.

It is obvious that the reinforced honeycombs behave similar to metallic materials rather than brittle plastics, and this finding is consistent with the aforementioned mechanical behavior. The significant increase in strength can be attributed to the fact that the opposing cell walls will contact each other earlier under greater relative density, after which the buckling of the cell walls stops, and further deformation mainly occurs in the material itself rather than in the honeycomb structure.

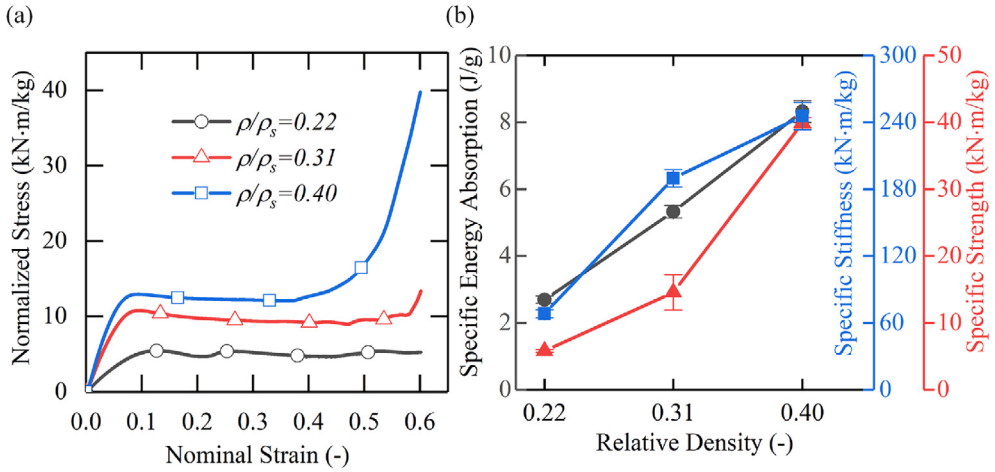

Fig. 7. Mechanical response of reinforced honeycombs with different relative densities: (a) normalized stress–strain curves of reinforced honeycombs with different relative densities and (b) influence of relative density on the mechanical properties of reinforced honeycombs.

3.1.3. Influence of carbon fiber content on the mechanical performance

Carbon fiber content has a significant effect on the mechanical performance of reinforced honeycombs. According to Eq. (2), specimens were prepared with different layer heights (0.2 mm, 0.3 mm, and 0.4 mm) and constant relative densities of 0.31. The smaller the layer height was, the longer the total printing path needed, and the greater number of carbon fibers used; therefore, when the layer height increased from 0.2 mm to 0.4 mm, the carbon fiber content decreased from about 20% to 10%. Fig. 8(a) shows an evident densification of honeycomb with 20% fiber content. In comparison, the stress increase is much smaller in honeycombs with lower fiber content, even though the initial strain of the densification stage is approximately equal. This phenomenon occurs because of the enhancement effect of carbon fibers on the composite material, which is another way to significantly improve the ultimate strength of honeycomb. Fig. 8(b) shows that when the carbon fiber content increased from 10% to 20%, the specific strength of the reinforced honeycombs varied from 11.52 kN · m/kg to 30.39 kN · m/kg, the specific stiffness increased from 160.12 kN · m/kg to 254.50 kN · m/kg, and the SEA increased from 4.82 J/g to 6.86 J/g. As expected, the maximum value (254.50 kN · m/kg, 30.39 kN · m/kg and 6.86 J/g) is obtained by the specimens with 20% fiber content, which means that the carbon fiber plays a main role in the mechanical performance of reinforced honeycombs.

3.2. Failure mode of honeycombs under compressive loading

For conventional honeycombs, the decrease in stress after reaching the peak stress corresponds to the buckling of the inclined cell wall, as shown in Fig. 9(a,b). At a certain deformation level, a local, brittle fracture will occur at the junction between the inclined and vertical cell wall. The onset of fracture results in an abrupt drop in the stress level; this fracture follows the increasing stress as the inclined cell walls contact the vertical walls. In contrast, the carbon fiber reinforcement can prevent the cell wall fracture until contact is made with the other walls. This mechanism may explain the unique mechanical behavior of reinforced honeycombs under longitudinal compression (a plateau in stress–strain curve) and enables honeycombs to maintain their structural integrity. We note that the failure modes of reinforced

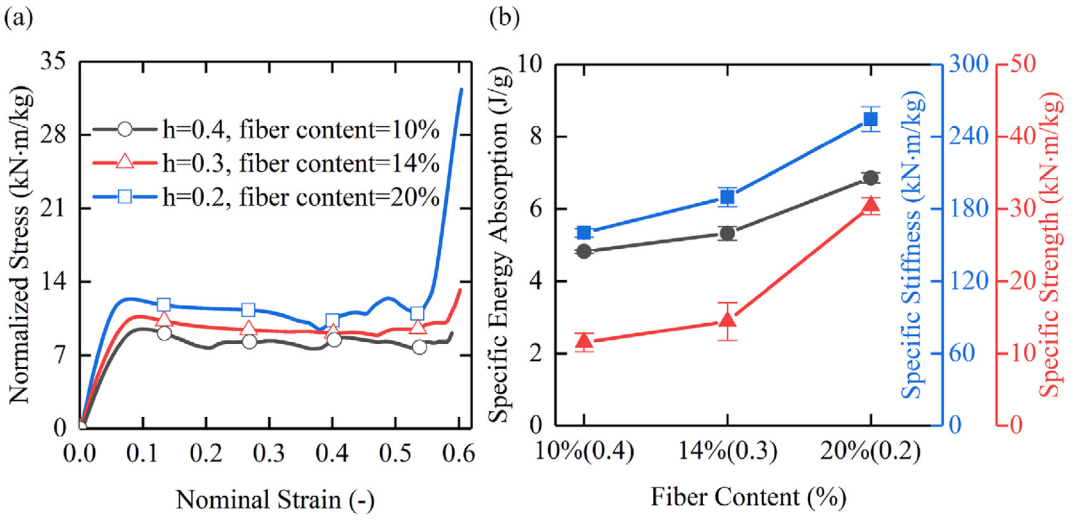

Fig. 8. Mechanical response of reinforced honeycombs with different fiber contents: (a) normalized stress–strain curves of reinforced honeycombs with different fiber contents and (b) influence of fiber content on the mechanical properties of reinforced honeycombs.

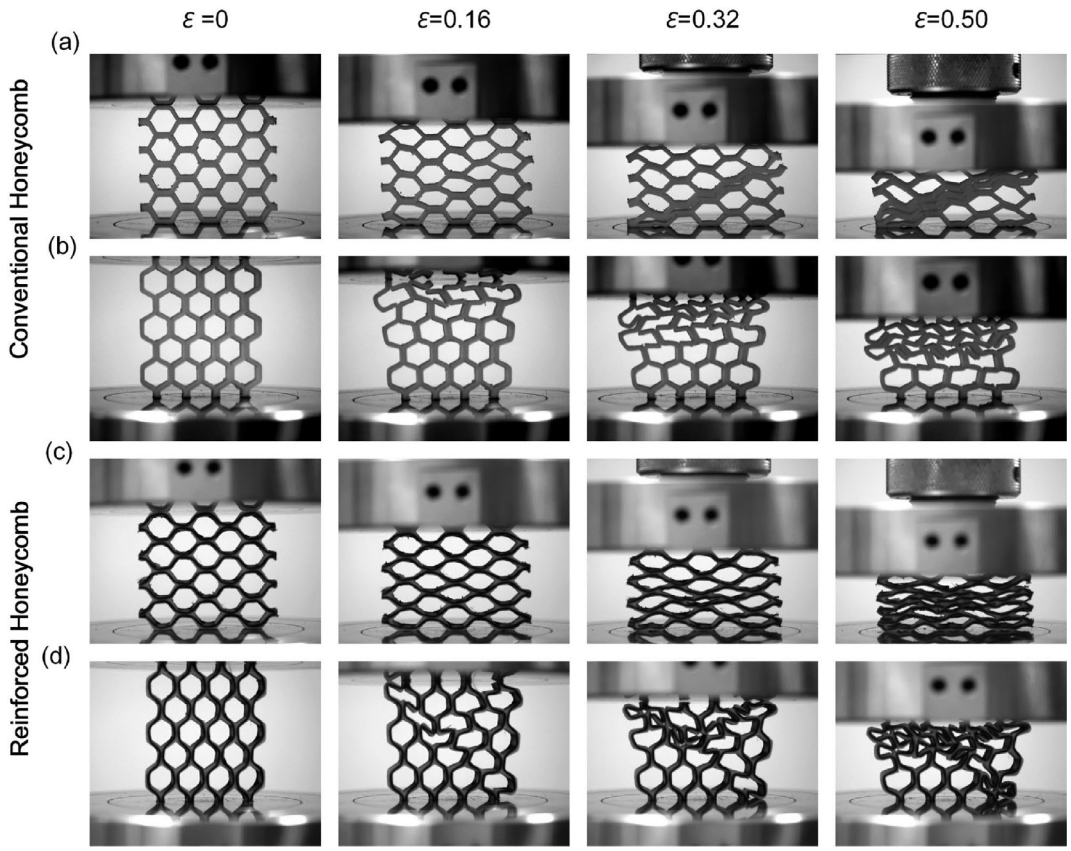

Fig. 9. Behaviors of honeycombs under large compression: (a)-(b) conventional honeycombs under longitudinal and transverse loads and (c)-(d) carbon fiber-reinforced honeycombs under longitudinal and transverse loads.

honeycombs are different under different loading directions. Fig. 9(c, d) shows that unlike the desirable global deformation observed in reinforced honeycomb under longitudinal loading, the reinforced honeycombs under transverse loading exhibit local, shear failure under large deformation, which is the same behavior exhibited by the conventional honeycombs.

This phenomenon can be explained by the different load-carrying conditions of carbon fibers. In the longitudinal loading case, the inclined cell walls serve as a plastic hinge, which bends outward after the yield point; this behavior means that the inclined cell walls and vertical cell walls are flattened, and the opposing inclined cell walls gradually touch the adjacent walls. Hence, carbon fibers experience tensile loading along their longitudinal direction, for which their excellent strength is fully utilized. In the transverse loading case, however, the inclined cell walls bend inward, and opposing cell walls move away from each other. Fig. 9(d) shows that the brittle fracture of the matrix can easily propagate at the junction between adjacent inclined cell walls, and the carbon fiber cannot effectively inhibit the formation of fracture, which causes the reinforced honeycomb to behave similar to a brittle plastic under transverse loading. The primary reason for a totally different compression response under the transverse loading is that the direction of carbon fiber is longitudinal rather than transverse direction.

Fig. 10 shows a comparison of reinforced honeycombs under different loading directions. Fig. 10(a,b) shows the reinforced honeycombs under the compression load in different directions. CT scans were performed to detect the fractures in these two kinds of specimen under longitudinal and transverse compression load. Fig. 10(c) shows a CT scan slice of the honeycomb structure after transverse compression test, and Fig. 10(d) shows a CT scan slice of the honeycomb structure after longitudinal compression test. The CT slices show that, when the reinforced honeycomb is subjected to transverse compression, the honeycomb is prone to brittle fracture at the junction of the vertical edges and inclined edges; whereas, when the honeycomb is under longitudinal loading, the structure could maintain much better integrity, there was almost no obvious fracture occurred. Fig. 10(e,f) show the SEM pictures of the tension failure of a 3D printed continuous carbon fiber reinforced composite specimen for tensile testing. Here, the exposed carbon fibers can be seen clearly, indicating that the carbon fiber and the matrix were not completely impregnated during the printing process, and the strengthening effect of carbon fibers would be reduced.

3.3. Self-heating and self-healing effects of carbon fiber-reinforced honeycombs

Shape memory polymers (SMPs) are a class of smart materials that can regain its original shape under external stimuli such as temperature, light, electric current, magnetic field. While the current work does not investigate the fundamental phenomenon, but rather employs for additional structure functionalities; interested readers are referred to the numerous works on various SMP including photo-cured poly (D,L-lactide) dimethacrylate networks, carbon fiber reinforced shape memory beam and SMP applications in medical field [47–55].

In this section, we illustrate the functional ability of the reinforced structure to recover the original shape after compression. The shape recovery is triggered by a low voltage excitation, which heats the carbon fibers, subsequently triggering the shape memory effect in the polymeric matrix.

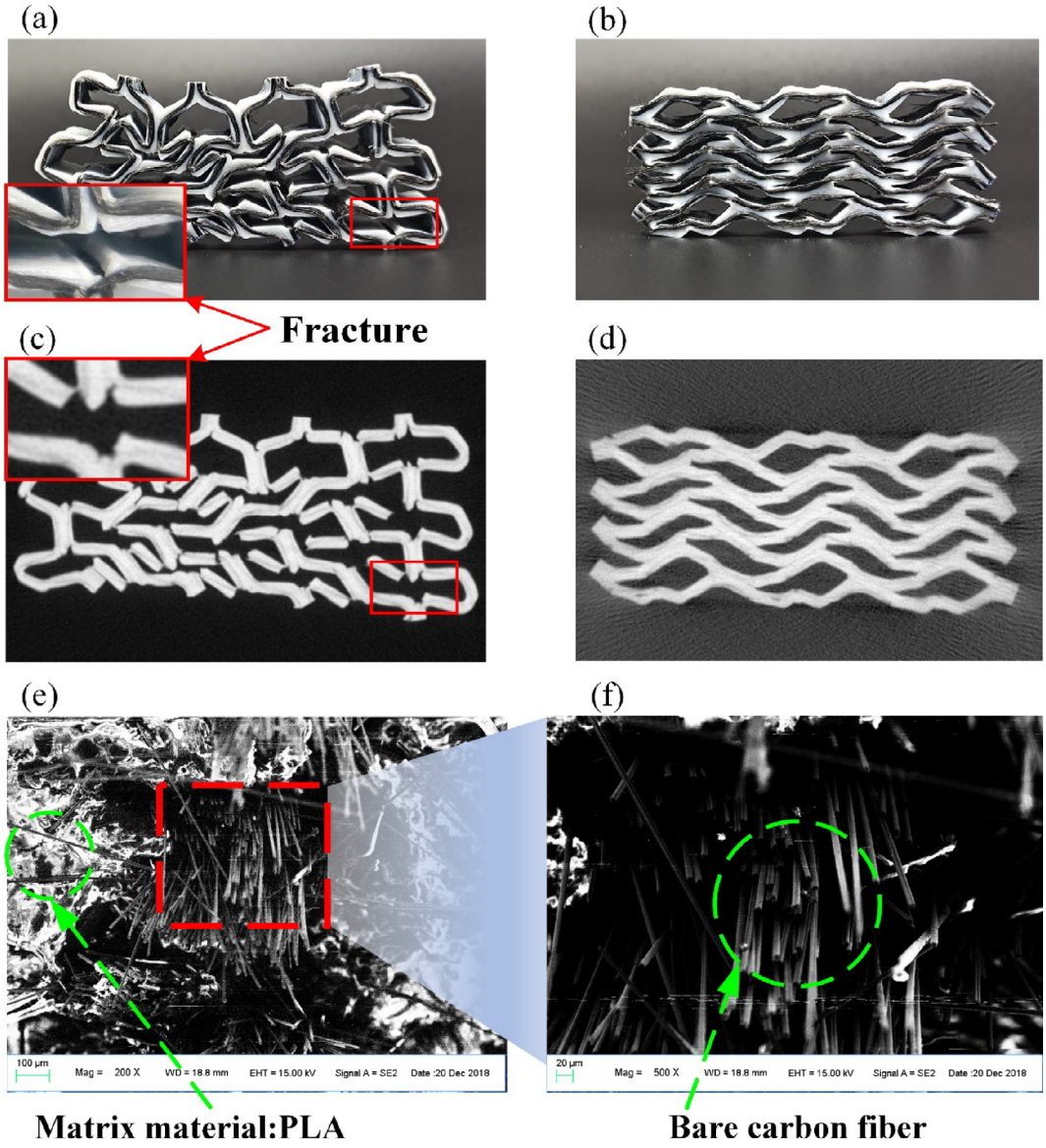

Fig. 10. Carbon fiber-reinforced honeycombs after longitudinal and transverse compression ($\varepsilon = 0.35$): (a) carbon fiber-reinforced honeycombs after transverse compression and (b) carbon fiber-reinforced honeycombs after longitudinal compression; (c) CT scan slice of the honeycomb structure after transverse compression;(d) CT scan slice of the honeycomb structure after longitudinal compression; (e) SEM picture of the tension failure of a 3D printed continuous carbon fiber reinforced composite specimen for tensile testing; (f) Local area SEM picture of the tension failure.

3.3.1. Recoverability of the 3D-printed carbon fiber-reinforced composite element

One segment of the 3D-printed carbon fiber-reinforced composite element was used to investigate the recoverability of the overall 3D-printed carbon fiber-reinforced composite. Fig. 11(a) shows that the PLA matrix material on both ends of the printed segment was removed. With the help of a cylinder, the printed segment was bent into a "C" shape, as shown in Fig. 11(b). Then, a 5 V voltage was applied to the "C" shape segment, as shown in Fig. 11(c). Fig. 11(d) shows that the "C" shape segment recovered its original straight shape in approximately 5 s, which means that under thermal stimulation, the 3D-printed carbon fiber-reinforced PLA composite exhibits good and fast recoverability.

3.3.2. Self-heating of carbon fiber-reinforced honeycombs

During the experiment, the carbon fiber served as both a reinforcement and an electrical heater, and the resistance of reinforced honeycomb was measured to be approximately 4 Ω. An obvious temperature increase can be observed under an applied voltage of 5 V. To record the heat distribution in the honeycombs, an infrared thermal imager (FLUKE Ti400®) was used during the experiment. Fig. 12(b) depicts the heating process of the reinforced honeycombs. The infrared image shows that the temperature reached approximately 40 °C after 30 s, and the temperature distribution was not even at the beginning due to the contact resistance. Then, a more uniform temperature distribution was observed as the heating time and average honeycomb temperature increased. After being subjected to the applied voltage for 5 min, the honeycomb temperature reached a maximum value of 120 °C and remained approximately constant.

3.3.3. Self-healing of carbon fiber-reinforced honeycombs

In the honeycomb structure, PLA is characterized by the coexistence of two different phases: the crystalline phase and amorphous phase. The crystalline region allows the PLA to recover its original

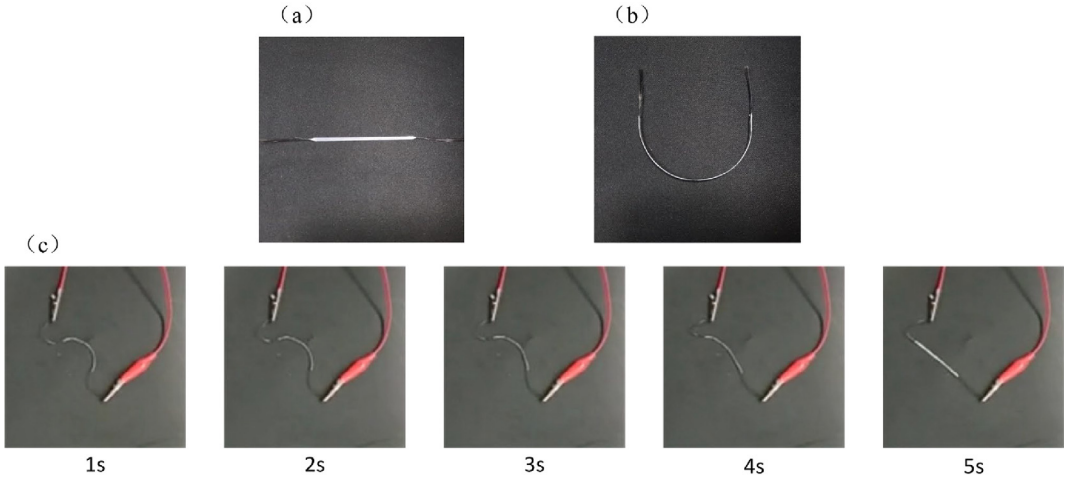

Fig. 11. Recoverability of the 3D-printed continuous carbon fiber-reinforced PLA composite element: (a) a single 3D-printed composite segment with PLA removed at both ends, (b) bending the segment into a "C" shape,(c) the recovery of the original straight shape in approximately 5 s under the 5 V excitation to the "C" shape segment.

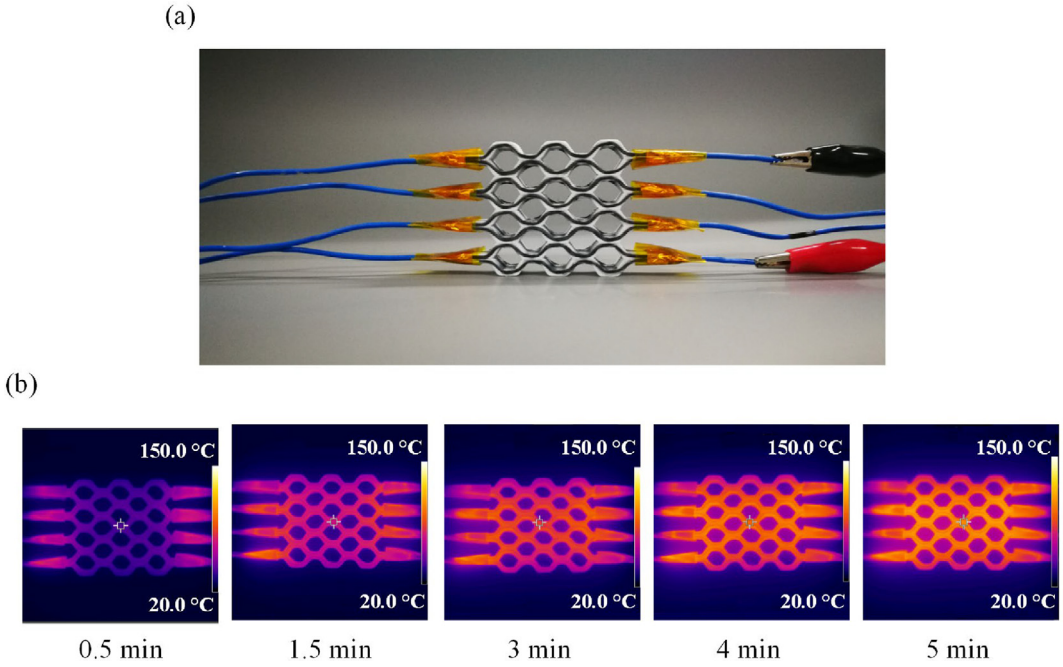

Fig. 12. Fabrication of self-heating carbon fiber-reinforced honeycomb: (a) the setup for self-heating carbon fiber-reinforced honeycombs and (b) the heating process of the reinforced honeycombs under an applied voltage of 5 V.

shape to some extent at certain temperatures, so PLA may function similar to shape memory polymers (SMPs). The main obstacle of using the shape memory effect of PLA in a functional structure is that the structure may fail due to fracture prior to recovery. Fortunately, carbon fibers can inhibit the formation of fractures in such structures even under large deformations. Hence, self-healing carbon fiber-reinforced honeycombs are realizable because of their shape integrity and self-heating effects. In this section, the relative density and fiber content of reinforced honeycombs are about 0.40 and 14% (0.3 mm layer height), respectively, and experiments are executed under two compressive strains: 0.2 and 0.45.

To measure the recovery effects of reinforced honeycombs, the shape recovery ratio was introduced in this study as follows:

$R_r = \frac{\varepsilon_m - \varepsilon_p}{\varepsilon_m} \times 100\%$, where, ε_m is the certain compression strain (0.2 and 0.45 in this paper),ε_p is the strain after recovery.

Fig. 13(a,b) shows that the honeycombs have a fairly good recovery ratio after the first loading, which is 87%. Fig. 13(e) shows the recovery process of reinforced honeycombs after applying a 5 V voltage, and the honeycombs can obviously recover close to their original shape. However, the recovery ratio decreases with increasing loading cycles and ultimately tends to maintain a constant value of 60%. The incomplete and diminishing recovery is mainly attribu-

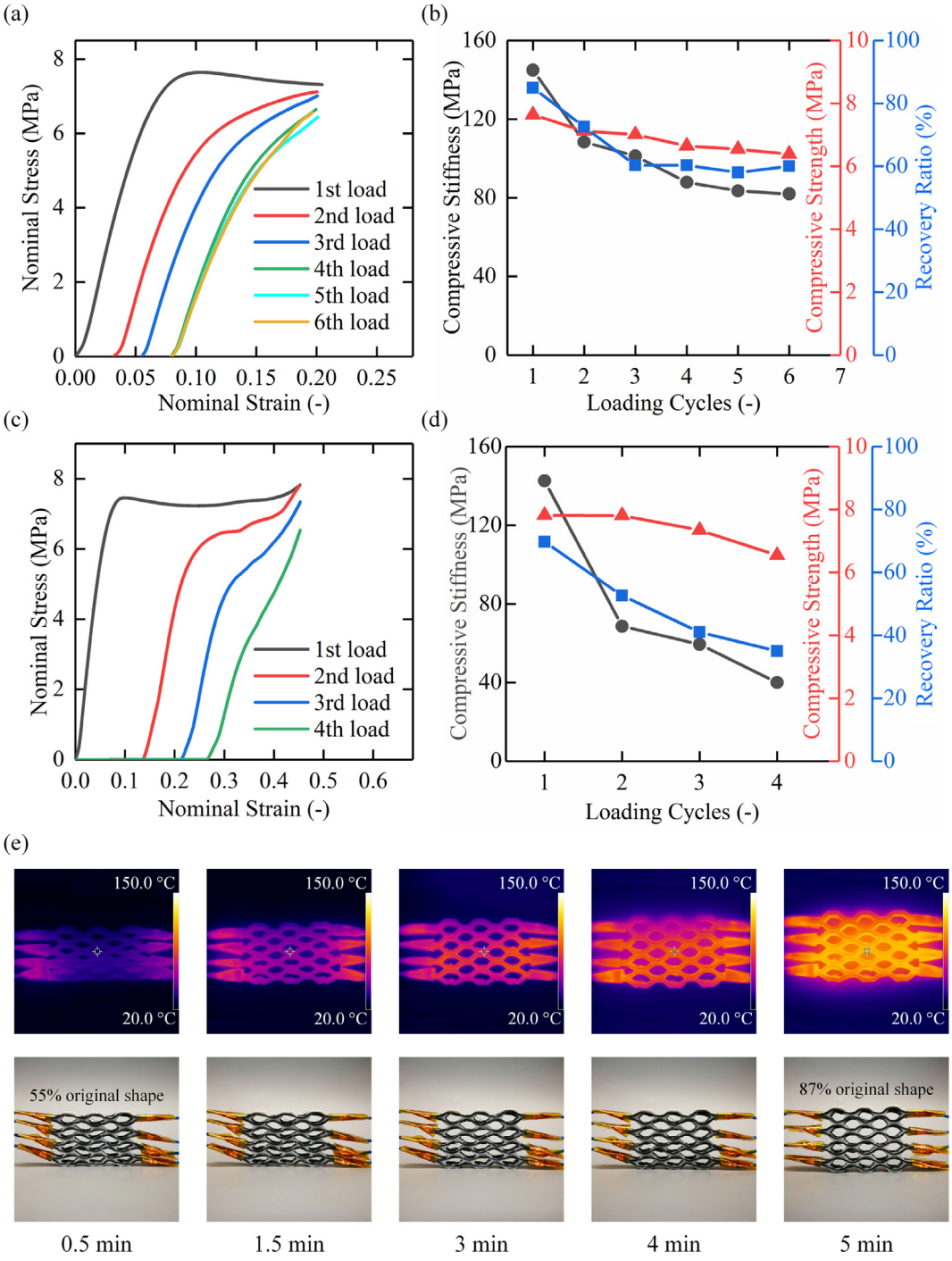

Fig. 13. Mechanical response of carbon fiber-reinforced honeycombs during several loading-recovery processes: (a-b) Mechanical responses of reinforced honeycomb with a compression strain up to 0.2, (c-d) mechanical response of reinforced honeycomb with a compression strain up to 0.45, and (e) recovery process of the reinforced honeycombs after large deformation.

ted to the irreversible effect of PLA, i.e., not all energy stored during plastic deformation can be released. Similar to the tendency of the recovery ratio, the compressive stiffness and compressive strength decrease from 114.92 MPa to 82 MPa and 7.64 MPa to 6.39 MPa, respectively. For larger deformation levels (strain of 50%), the irreversible effect is more obvious, as shown in Fig. 12 (c,d), wherein the recovery ratio decreases to 40% hence, there are fewer total loading cycles under larger deformation than under smaller deformation. After the first recovery, the stiffness of the honeycomb dropped steeply by approximately 50%, and then as the number of loading-recovery cycles increased, the stiffness slightly decreased. After the 4th loading, the stiffness of the honeycomb was just 40 MPa. Moreover, the compressive strength slightly decreased from 7.82 MPa to 6.54 MPa.

4. Conclusion

In this paper, we have presented a lightweight, strong, recoverable 3D-printed honeycomb composite with remarkable energy absorption properties. The continuous carbon fiber-reinforced honeycomb exhibits extraordinary mechanical properties under large compression. The SEA and specific stiffness of the reinforced honeycombs are 1–2 times higher than those of conventional honeycombs, and interestingly, due to the anisotropy of carbon fibers, the mechanical properties are entirely distinct along different loading directions. When under longitudinal compression, the continuous carbon fiber-reinforced honeycomb composite structure exhibits a stable 3-stage (linear elasticity-plateau-densification) stress–strain curve that is similar to that of metallic honeycomb structures. Our experiments show that the specific strength, specific stiffness and SEA are closely related to the relative density and carbon content. This realization provides a way to tailor the mechanical properties of 3D-printed honeycombs by adjusting these parameters.

To further demonstrate the properties of carbon fiber-reinforced honeycombs, we also studied their self-heating and self-healing effects. The results show that the reinforced honeycomb can be heated from ambient temperature to 120 °C in 5 min under an applied voltage of 5 V. Furthermore, the reinforced honeycomb shows good recoverability due to the thermally induced polymer shape memory effect, even when the deformation from longitudinal compression is large (strain of approximately 20%–50%). In this study, carbon fiber-reinforced honeycombs are made from the most common commercial PLA filament, which is brittle and insufficient in shape memory. Many alternative materials can be chosen as a matrix. Therefore, the findings of this paper not only provide a new way to enhance the mechanical properties of honeycomb but also provide insight into controllable shape memory applications. Moreover, 3D printed continuous carbon fibers reinforced structures with complex continuous fiber arrangements can provide additional ways for achieving tailored mechanical properties. Furthermore, adoption of alternative matrix blends such as PLA/TPU can potentially increase the recoverability of the 3D printed honeycomb structure. Finally, we note that important issue of the wettability that can be improved through, for example, carbon fiber modification [27], selecting better processing parameters [56], optimizing the printing nozzle structure [57], and, thus, can contribute to further enhancement of the mechanical properties of the 3D printed composite structures.

Declaration of Competing Interest

The authors declare that they have no known competing financial interests or personal relationships that could have appeared to influence the work reported in this paper.

Acknowledgments

The authors acknowledge support from the Overseas Famous University Visiting Plan of Northwestern Polytechnical University for the first author's visit to the University of Wisconsin-Madison. The mechanical testing of the 3D-printed honeycomb specimens was conducted at the Material Testing and Analysis Center of Shaanxi Province, China.

Appendix A

Relative density is defined as the ratio of the density of the honeycomb to the density of the matrix material, formula (1) is deduced as below:

$$\rho = \frac{M_h}{V_h} \tag{A.1}$$

$$M_h = \rho_s V_s \tag{A.2}$$

$$\Delta\rho = \frac{\rho}{\rho_s} \tag{A.3}$$

where, $\Delta\rho$, ρ and ρ_s are relative density, density of the honeycomb and the density of the matrix respectively. M_h and V_h represent the weight and volume of the honeycomb, V_s is the volume of solid material.

Then, Eq. (A.3) can be transformed as follows,

$$\Delta\rho = \frac{V_s}{V_h} \tag{A.4}$$

$$V_s = H(2ht_1 + 4lt_2) \tag{A.5}$$

$$V_h = H(2l\sin\theta \times (2h + 2l\cos\theta)) \tag{A.6}$$

$$\Delta\rho = \frac{ht_1 + 2lt_2}{2hl\sin\theta + l^2\sin 2\theta} \tag{A.7}$$

Therefore, the relative density is the ratio of the volume of the solid part to the total volume of the whole honeycomb, because of the same thickness, the result can be obtained by calculating the area ratio instead of volume according to the basic parameters in Fig. 3(b).

References

[1] Roderic Lakes. Materials with structural hierarchy. Nature, volume 361, pages 511–515 (11 February 1993)
[2] Lorna J. Gibson, Michael F. Ashby. Cellular Solids: Structure and Properties. Cambridge University Press, July, 1999.
[3] Evans AG, Hutchinson JW, Fleck NA, Ashby M, Wadley H. The topological design of multifunctional cellular metals. Prog Mater Sci 2001;46:309.
[4] Wadley HN, Fleck NA, Evans AG. Fabrication and structural performance of periodic cellular metal sandwich structures. Compos Sci Technol 2003;63:2331.
[5] Zheng L, Wu D, Zhou A, Pan B, Wang Y, Wang J. Experimental and numerical study on heat transfer characteristics of metallic honeycomb core structure in transient thermal shock environments. Int J Thermophys 2014;35:1557.
[6] Chen Q, Cao P-F, Advincula RC. Mechanically robust, ultraelastic hierarchical foam with tunable properties via 3D Printing. Adv Funct Mater 2018;1800631.
[7] T. A. Schaedler, A. J. Jacobsen, A. Torrents, A. E. Sorensen etc. Ultralight Metallic Microlattices. Science, vol 334, 18 Nov 2011
[8] Minas C, Carnelli D, Tervoort E, Studart AR. 3D printing of emulsions and foams into hierarchical porous ceramics. Adv Mater 2016;28:9993–9.
[9] Hedayati R, Sadighi M, Mohammadi Aghdam M, Zadpoor AA. Mechanical properties of additively manufactured thick honeycombs. Materials (Basel) 2016;9:613.
[10] Zhang P, Arceneaux DJ, Khattab A. Mechanical properties of 3D printed polycaprolactone honeycomb structure. J Appl Polym Sci 2018;135(12).
[11] Biranchi Panda, Marco Leite, Bibhuti Bhusan Biswal, Xiaodong Niu, Akhil Garg. Experimental and numerical modelling of mechanical properties of 3D printed honeycomb structures [J]. Measurement, 2018, 116.
[12] Shengyu Duan, Yong Tao, Hongshuai Lei, Weibin Wen, Jun Liang, Daining Fang. Enhanced out-of-plane compressive strength and energy absorption of 3D printed square and hexagonal honeycombs with variable-thickness cell edges. Extreme Mechanics Letters, 2018, 18.
[13] Habib FN, Iovenitti P, Masood SH, et al. In-plane energy absorption evaluation of 3D printed polymeric honeycombs. Virtual Phys Prototyping 2017:1–15.
[14] Bates SRG, Farrow IR, Trask RS. Compressive behaviour of 3D printed thermoplastic polyurethane honeycombs with graded densities. Mater Des 2018.
[15] Chen Y, Li T, Jia Z, Scarpa F, Yao C-W, Wang L. 3D printed hierarchical honeycombs with shape integrity under large compressive deformations. Mater Des 2018;137:226–34.
[16] Boopathy VR, Sriraman A, Arumaikkannu G. Energy absorbing capability of additive manufactured multi-material honeycomb structure. Rapid Prototyping J 2019;25(3).
[17] Fijul Kabir SM, Mathur K, Seyam A-F. A critical review on 3D printed continuous fiber-reinforced composites: History, mechanism, materials and properties. Compos Struct 2020;232.
[18] Goh GD, Yap YL, Agarwala S, et al. Recent progress in additive manufacturing of fiber reinforced polymer composite. Adv Mater Technol 2018.
[19] Quan Z, Wu A, Keefe M, et al. Additive manufacturing of multi-directional preforms for composites: opportunities and challenges. Mater Today 2015;18(9):503–12.
[20] Parandoush P, Lin D. A review on additive manufacturing of polymer-fiber composites. Compos Struct 2017;182(15):36–53.
[21] van der Klift F, Koga Y, Todoroki A, Ueda M, Hirano Y, Matsuzaki R. 3D printing of continuous carbon fibre reinforced thermo-plastic (CFRTP) Tensile Test Specimens. Open J Compos Mater 2016;6:18–27.

[22] Melenka GW, Cheung BKO, Schofield JS, Dawson MR, Carey JP. Evaluation and prediction of the tensile properties of continuous fiber-reinforced 3D printed structures. Compos Struct 2016;153:866–75.
[23] Dickson AN, Barry JN, McDonnell KA, Dowling DP. Fabrication of continuous carbon, glass and Kevlar fibre reinforced polymer composites using additive manufacturing. Addit Manuf 2017;16:146–52.
[24] Goh GD, Dikshit V, Nagalingam AP, Goh GL, Agarwala S, Sing SL, et al. Characterization of mechanical properties and fracture mode of additively manufactured carbon fiber and glass fiber reinforced thermoplastics. Mater Des 2018;137:79–89.
[25] Justo J, Távara L, García-Guzmán L, París F. Characterization of 3D printed long fibre reinforced composites. Compos Struct 2018;185:537–48.
[26] Matsuzaki R, Ueda M, Namiki M, Jeong T-K, Asahara H, Horiguchi K, et al. Three-dimensional printing of continuous-fiber composites by in-nozzle impregnation. Sci Rep 2016;6:1–7.
[27] Li N, Li Y, Liu S. Rapid prototyping of continuous carbon fiber reinforced polylactic acid composites by 3D printing. J Mater Process Technol 2016;238:218–25.
[28] Yu T, Ren J, Li S, Yuan H, Li Y. Effect of fiber surface-treatments on the properties of poly(lactic acid)/ramie composites. Compos Part A Appl Sci Manuf 2010;41:499–505.
[29] Tian X, Liu T, Yang C, Wang Q, Li D. Interface and performance of 3D printed continuous carbon fiber reinforced PLA composites. Compos Part A Appl Sci Manuf 2016;88:198–205.
[30] Yang C, Tian X, Liu T, Cao Y, Li D. 3D printing for continuous fiber reinforced thermoplastic composites: mechanism and performance. Rapid Prototyp J 2017;23:209–15.
[31] Tian X, Liu T, Wang Q, Dilmurat A, Li D, Ziegmann G. Recycling and remanufacturing of 3D printed continuous carbon fiber reinforced PLA composites. J Clean Prod 2017;142:1609–18.
[32] Hou Z, Tian X, Zhang J, Li D. 3D printed continuous fibre reinforced composite corrugated structure. Compos Struct 2018;184:1005–10.
[33] Sugiyama K, Matsuzaki R, Ueda M, Todoroki A, Hirano Y. 3D printing of composite sandwich structures using continuous carbon fiber and fiber tension. Compos A Appl Sci Manuf 2018;113:114–21.
[34] Vishwesh Dikshit, Arun Prasanth Nagalingam, Guo Dong Goh, Shweta Agarwala, Wai Yee Yeong, Jun Wei. Quasi-static indentation analysis on three-dimensional printed continuous-fiber sandwich composites. Journal of Sandwich Structures and Materials, 2019.
[35] Funari MF, Greco F, Lonetti P. Sandwich panels under interfacial debonding mechanisms. Compos Struct 2018;203(1):310–20.
[36] Fabrizio Greco, Paolo Lonetti, Raimondo Luciano, Paolo Nevone Blasi, Andrea Pranno. Nonlinear effects in fracture induced failure of compressively loaded fiber reinforced composites. Composite Structures, Volume 189, 1 April 2018, Pages 688-699
[37] Greco F, Leonetti L, Pranno A, Rudykh S. Mechanical behavior of bio-inspired nacre-like composites: A hybrid multiscale modeling approach. Compos Struct February 2020;233(1):111625.
[38] Xie T. Tunable polymer multi-shape memory effect. Nature 2010;464:11.
[39] Tao R, Yang Q-S, Zhang X-J, Liu X, He X-Q, Liew K-M. Numerical study of smart honeycomb core using shape memory polymers. J Appl Polym Sci 2017;45672:45672.
[40] Huang J, Zhang Q, Scarpa F, Liu Y, Leng J. Shape memory polymer-based hybrid honeycomb structures with zero Poisson's ratio and variable stiffness. Compos Struct 2017;179:437–43.
[41] Zarek M, Layani M, Cooperstein I, Sachyani E, Cohn D, Magdassi S. 3D printing of shape memory polymers for flexible electronic devices. Adv Mater 2016;28:4449–54.
[42] Zhang W, Chen L, Zhang Y. Surprising shape-memory effect of polylactide resulted from toughening by polyamide elastomer. Polymer (Guildf) 2009;50:1311–5.
[43] Lai SM, Wu WL, Wang YJ. Annealing effect on the shape memory properties of polylactic acid (PLA)/thermoplastic polyurethane (TPU) bio-based blends. J Polym Res 2016;23:2–9.
[44] Jing X, Mi H-Y, Peng X-F, Turng L-S. The morphology, properties, and shape memory behavior of polylactic acid/thermoplastic polyurethane blends. Polym Eng Sci 2015;55:70–80.
[45] Mao Y, Kai Yu, Isakov MS, Jiangtao Wu, Dunn ML, Jerry Qi H. Sequential self-folding structures by 3D printed digital shape memory polymers. Sci Rep 2015;5:13616.
[46] Yang C, Wang B, Li D, et al. Modelling and characterization for the responsive performance of CF/PLA and CF/PEEK smart materials fabricated by 4D printing. Virtual Phys Prototyping 2017;12(1):69–76.
[47] Wang Y, Liu J, Xia L, Shen M, Xin Z. Super-tough poly(lactic acid) thermoplastic vulcanizates with heat triggered shape memory behaviors based on modified natural Eucommia ulmoides gum. Polym Test 2019;80.
[48] Zeng C, Liu L, Bian W, Liu Y, Leng J. 4D printed electro-induced continuous carbon fiber reinforced shape memory polymer composites with excellent bending resistance. Compos Part B Eng 2020;194..
[49] Herath M, Epaarachchi J, Islam M, Fang L. Leng J. Light activated shape memory polymers and composites: A review. Eur Polym J; 2020. p. 136.
[50] Fu S, Chen S. Shape memory polyurethanes with UV light-triggered deformation and water-induced recovery. Mater Today Proc 2019;16..
[51] Zamani Alavijeh R, Shokrollahi P, Barzin J. A thermally and water activated shape memory gelatin physical hydrogel, with a gel point above the physiological temperature, for biomedical applications. J Mater Chem B 2017;5..
[52] Cui X, Chen J, Zhu Y, Jiang W. Natural sunlight-actuated shape memory materials with reversible shape change and self-healing abilities based on carbon nanotubes filled conductive polymer composites. Chem Eng J 2020.
[53] Liu R, Xu S, Luo X, Liu Z. Theoretical and numerical analysis of mechanical behaviors of a metamaterial-based shape memory polymer stent. Polymers (Basel) 2020;12.
[54] Di Bartolo A, Melchels FPW. Prolonged recovery of 3D printed, photo-cured polylactide shape memory polymer networks. APL Bioeng 2020;4:036105.
[55] Lee SH, Kim SW. Self-sensing-based deflection control of carbon fibre-reinforced polymer (CFRP)-based shape memory alloy hybrid composite beams. Compos Struct 2020;251:1–13.
[56] Chacón JM, Caminero MA, García-Plaza E, Núñez PJ. Additive manufacturing of PLA structures using fused deposition modelling: Effect of process parameters on mechanical properties and their optimal selection. Mater Des 2017;124:143–57.
[57] Hardikkumar Prajapati, Swapnil S. Salvi, Darshan Ravoori, Momen Qasaimeh, Ashfaq Adnan, Ankur Jain. Improved print quality in fused filament fabrication through localized dispensing of hot air around the deposited filament. Additive Manufacturing, Volume 40, 2021,101917.